



# Recycling of fine fraction of spent foundry sands into fireclay bricks

Volha Zalyhina<sup>1</sup> · Victoria Cheprasova<sup>1</sup> · Valentin Romanovski<sup>2</sup>

Received: 10 March 2023 / Accepted: 28 September 2023 / Published online: 19 October 2023  
© The Author(s), under exclusive licence to Springer Nature Japan KK, part of Springer Nature 2023

## Abstract

The most large-scale foundry waste is burnt molding earth, which is formed at the stage of knocking out castings from foundry molds. The properties of burnt molding earth (humidity, loss on ignition, elemental, phase, and grain composition) were studied and the possibility of its regeneration was confirmed. It is shown that during mechanical regeneration, about 24 wt.% of the considered waste turns into a fine pulverized fraction, which cannot be returned to the technological process and is sent to a landfill. On the basis of experimental studies, it has been established that this fraction of burnt molding earth can be used in the production of ceramic bricks as a lean additive. The obtained samples of ceramic bricks containing 20 wt.% finely dispersed fraction of molding burnt earth at a firing temperature of 1000 °C for 60 min are characterized by the following properties: average density 2020 kg/m<sup>3</sup>, water absorption 10.8%, compressive strength 39.8 MPa, and ultimate strength in bending 12.67 MPa.

**Keywords** Waste · Burnt molding earth · Foundry production · Fine fraction · Water absorption · Compressive strength

## Introduction

Waste recycling is a very relevant issue and complied with the United Nations Sustainable Development Goal 12 which is about responsible consumption and production, prioritizing waste recycling, and waste reduction via sustainable innovation processes. Currently, mechanical engineering is one of the most important sectors of the economy in many countries. The largest specific share in the total volume of machine-building production is the automotive industry—54%. The electrical industry accounts for 16%; heavy and power engineering—8%; chemical and oil engineering—5%; road and municipal engineering—2.5%; and machine tool and instrument making—1.5% [1]. In all these industries, the main place is occupied by metallurgical production, which is a labor-intensive technological process.

The main stages of metallurgical foundry production are: metal smelting, mold making, casting metal into molds, knocking blanks out of molds, and cleaning blanks. The technological scheme of the foundry is shown in Fig. 1.

As can be seen from the scheme, in the foundry, such wastes as burnt molding earth, iron-containing dust, and metallurgical slags are generated. The most large-scale waste is spent foundry sand (SFS). SFS or burnt molding earth is formed when metal castings are knocked out of molds. In Europe and the United States, respectively, the production of SFS is reaching 9 and 12 million metric tons per year, with disposal costs ranging from \$135 to \$657 million [2]. It is disposed of in landfills, although doing so puts the environment in danger and is not financially viable [3, 4]. According to the literature data, burnt molding earth consists of 90–95% quartz sand [5].

Currently, in most enterprises, SFS is subjected to regeneration in order to return it to the technological process at the stage of casting molds. Mechanical regeneration is usually used as the simplest and cheapest way. However, in this case, a finely dispersed fraction is formed, which cannot be reused for the manufacture of casting molds and is transported to a landfill. The search for the best ways to dispose of SFS is still relevant. The use of wastes in the production of building materials is widely known: wood fiber and milled glass [6], walnut shell waste [7, 8], waste lime mud [9, 10], paper

✉ Volha Zalyhina  
zalyhina@mail.ru

✉ Valentin Romanovski  
rvd9ar@virginia.edu

<sup>1</sup> Department of Industrial Ecology, Belarusian State Technological University, Sverdlova, 13a, 220006 Minsk, Belarus

<sup>2</sup> Department of Materials Science and Engineering, University of Virginia, Charlottesville, VA 22904, USA

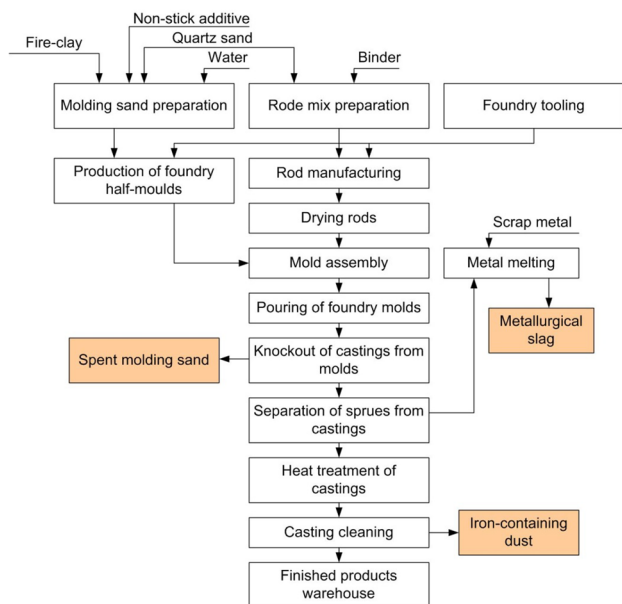


**Fig. 1** Technological scheme of foundry production

industry slag [11], water treatment sediments and spent sulfuric acid [12–14], paper waste [15], spent aluminum and rice husk [16], bamboo-fiber [17] and kenaf fiber [18], wig fiber [19], galvanic wastes [20–24], electric arc furnace dust [25], municipal sewage sludge [26], and mining wastes [27–29]. The latest published results consider the use of SFS in the production of cement [30, 31], ceramic materials [32, 33], and road construction [34, 35].

Among the production of ceramic materials, one of the promising options is the use of SFS instead of sand in the production of ceramic bricks [36]. However, when analyzing publications on the use of SFS in the production of ceramic bricks, we did not find publications and a wide range of basic parameters of bricks obtained by replacing sand with SFS. The formulations mentioned in the publications contain SFS in combination with other additives. At the same time, it should be said that the reuse of SFS to obtain molds is used after regeneration, including grinding and magnetic separation. However, this produces a significant amount of SFS fines, which cannot be used to produce injection molds as required.

The purpose of this work is to develop the most rational method for processing the fine pulverized fraction of the molding SFS.

## Materials and methods

### Materials and reagents

Based on an analytical review of published research, it is proposed to use a finely dispersed fraction of the molding SFS in

**Table 1** Compositions of samples of ceramic bricks, wt. %

Clay	Quartz sand	Finely dispersed fraction of SFS
80	20	–
80	15	5
80	10	10
80	5	15
80	–	20

the production of ceramic bricks. To study the possibility of obtaining ceramic bricks using SFS, prototypes were obtained in the work. Clay, quartz sand, and burnt molding earth were used for synthesis. Clay was characterized by the following composition (in terms of oxides, wt. %): SiO<sub>2</sub>—50.44, Al<sub>2</sub>O<sub>3</sub>—17.69, TiO<sub>2</sub>—0.92, Fe<sub>2</sub>O<sub>3</sub>—7.45, CaO—5.47, MgO—2.90, K<sub>2</sub>O—4.49, Na<sub>2</sub>O—0.68, loss on ignition—9.96.

Grinding of SFS was carried out on a planetary mill PM100-RETSCH. It was found that in this case about 24 wt. % fine dispersed fraction, the particles of which are characterized by a grain size of less than 190 μm. This fraction cannot be returned to the technological process for the manufacture of casting molds.

### Samples synthesis

Experimental samples of ceramic bricks were molded in a plastic way, followed by drying at a temperature of 105 °C and firing with isothermal exposure at a temperature of 850–1100 °C for a 30–120 min. The compositions of the studied samples are presented in Table 1.

### Samples analysis

X-ray phase analysis of the obtained samples was carried out on a D8 Advance X-ray diffractometer (Bruker AXS, Germany). The elemental composition and morphology of the burnt molding earth and obtained bricks samples were carried out on a JSM-5610 LV scanning electron microscope (JEOL, Japan).

Waste moisture content was determined in accordance with GOST 29234.5–91 “Moulding sands. Moisture Determination Method” by reducing the mass of the sample after drying in an oven at a temperature of 105–110 °C to constant weight. The mass fraction of moisture in percent (W) was calculated by the equation:

$$W = \frac{m_1 - m_2}{m_1} \cdot 100\%, \quad (1)$$

where  $m_1$ —the weight of the sample of SFS before drying, g;  $m_2$ —weight of the SFS sample after drying, g.

Loss on ignition was determined in accordance with GOST 29234.13–91 “Moulding sands. Method for determining the loss of mass on ignition” by reducing the mass of a sample upon ignition at a temperature of 1000 °C to constant mass. Mass fraction of weight loss on ignition ( $LI$ ) was calculated by the equation:

$$LI = \frac{m_1 - m_2}{m} \cdot 100\%, \quad (2)$$

where  $m_1$ —mass of the crucible with a sample before calcination, g;  $m_2$ —mass of the crucible with a sample after calcination, g;  $m$ —sample weight, g.

To study the grain composition of sand, sieve analysis was used according to GOST 29234.3-91 “Moulding sands. Method for determining the average grain size and uniformity coefficient”. Before testing, the sieves are stacked on top of each other in order of increasing sieve number from bottom to top. A bowl is provided at the bottom of the set of sieves. A set of sieves is installed on a special device, which, using an eccentric mechanism, shakes a stack of sieves in a horizontal plane with a frequency of 300 vibrations per minute. After sifting the sand for 15 min, the sieves are removed from the device and the remaining sand is weighed on each sieve and in the basin. The totality of the grains remaining on each sieve constitutes a separate fraction with particle sizes within the holes of the superior and this sieve.

The grain composition of sand is characterized by the average grain size, uniformity coefficient and specific surface area of the grains. The average grain size and uniformity coefficient are calculated from the results of sand sample sifting and the quantitative distribution of particles over sieves. The mass fraction of the residue on the sieve  $X_i$  is calculated by the following formula, %:

$$X_i = (m_i \times 100) / 100, \quad (3)$$

where  $i$ —sieve serial number;  $m_i$ —sieve residue weight, g;  $m$ —initial weight, g.

Next, build an integral curve on a logarithmic scale. To do this, the size of the sides of the cells of the grid  $d_i$  is plotted on the abscissa axis on a logarithmic scale, and on the ordinate axis on a linear scale—the percentage of the mass of particles with a size less than  $d_i$ .

The average grain size  $d_{av}$  corresponds to the boundary that divides the distribution of particles into two equal parts, i.e., characterizes the size of an imaginary sieve through which exactly 50% of the sand base would pass.

To determine the coefficient of uniformity from the integral curve, the percentage of particles smaller than  $4/3 \cdot d_{av}$

and  $2/3 \cdot d_{av}$  is found. The homogeneity coefficient is equal to the difference between these values.

The specific surface area ( $Sp$ ) was determined by the calculation method according to the equation [37]:

$$Sp = 22.64 \frac{\sum_i (\frac{m_i}{\delta_i})}{m}, \quad (4)$$

where  $i$ —sieve serial number;  $m_i$ —mass of individual sand fractions, g;  $m$ —mass of sand sample, g;  $\delta_i$ —characteristic grain size on a sieve, mm.

The characteristic grain size ( $\delta$ ) of each fraction was calculated by the equation:

$$\delta = (d + d_e) / 2, \quad (5)$$

where  $d$ —sieve mesh size, mm;  $d_e$ —mesh size of adjacent sieve above, mm.

The linear shrinkage of the samples was determined by measuring specially applied marks (marks 4 cm long) before and after heat treatment with a vernier caliper with an accuracy of  $\pm 0.01$  mm in accordance with ASTM C326-03.

Linear shrinkage  $LS$  (%) was determined by the following Eq. (6):

$$LS = \frac{L_0 - L \cdot 100}{L_0}, \quad (6)$$

where  $L_0$ —label initial size, mm;  $L$ —final label size, mm.

Apparent density was calculated by Eq. (7) (ASTM C373):

$$\rho = \frac{m}{V}, \quad (7)$$

where  $\rho$ —apparent density, g/cm<sup>3</sup>;  $m$ —mass of fired bricks, g;  $V$ —fired brick volume, cm<sup>3</sup>.

Water absorption ( $B$ ) was determined by Eq. (8) according to UNE-EN 772-11:

$$B = \frac{m - m_1}{m} \times 100\%. \quad (8)$$

The compressive strength of bricks ( $R$ ) was determined in accordance with GOST 530-2019 and UNE-EN 772-1 using the Eq. (9):

$$R = \frac{P}{F}, \quad (9)$$

where  $P$ —the maximum load established during the test of the sample, N;  $F$ —cross-sectional area of the sample, calculated as the arithmetic mean of the areas of its upper and lower surfaces, mm<sup>2</sup>.

Three samples in parallel were tested for each condition.

## Results and discussion

### Analysis of SFS

To select the most rational way of processing SFS, at the first stage, its properties were determined: moisture content, loss on ignition, elemental, phase and grain composition. It was found that the moisture content of SFS was 1.00–0.89%. Loss on ignition for SFS was 0.11–0.13%. It was also found that when calcined, the color of the SFS changes from gray–black to red–brown, which is associated with the content of iron in the SFS, when calcined, turns into iron oxide Fe<sub>2</sub>O<sub>3</sub>. The elemental composition of the studied foundry waste is presented in Table 2.

As can be seen from Table 2, the main elements of the SFS are Si and O; Al and Fe are also present in a noticeable amount. The study of the phase composition of SFS showed that in both cases the main phase is quartz – SiO<sub>2</sub> (Fig. 2a) with a hexagonal structure with space groups *P3221* and characteristic peak (101) at 26.64 2theta. Characteristic peaks of other phases like hematite were also found.

In the study of the grain composition of SFS, parameters such as the average grain size, homogeneity coefficient, and specific surface area were determined. To determine the grain composition, sieves with a hole diameter of 3 mm were used; 2 mm; 1 mm; 0.5 mm; 0.25 mm; 0.1 mm; 0.063 mm (Table 3).

As can be seen from the integral particle distribution curve,  $d_{av}$  was 0.35 mm. To determine the homogeneity coefficient, the integral curve was used to find the percentage of particles smaller than  $4/3 \cdot d_{av}$  ( $0.35 \times 4/3 = 0.47$ ) and  $2/3 \cdot d_{av}$  ( $0.35 \times 2/3 = 0.24$ ) in size. As can be seen from Fig. 2, the proportion of the mass of particles with a size smaller than the sides of a sieve cell  $4/3 \cdot d_{av}$  was 77%, and with a size smaller than the sides of a sieve cell  $2/3 \cdot d_{av}$ —15%. The homogeneity coefficient is equal to the difference between these values 62%.

$$Sp = 22.64 \frac{15158}{500} = 68.63 \text{ cm}^2/\text{g}.$$

Data on grain composition also correlate with particle sizes shown in SEM images (Fig. 2c).

Thus, the elemental and phase composition of the molding burnt earth confirm the possibility of its return to the technological process for the preparation of the molding sand for foundry molds after the removal of iron impurities, which is proposed to be carried out using electromagnetic separation. However, according to the granulometric composition, the burnt molding earth does not meet the requirements for it. Currently, operating enterprises for the manufacture of molding sands use medium sands of group 02 with a grain size of 190–230 μm with a specific surface area of at least 100 cm<sup>2</sup>/g. Therefore, to return the burnt molding earth to the technical process, it is necessary to grind it. When grinding, the binder films are also removed from quartz sand grains due to mechanical grinding of the mixture. The binder films are destroyed with the formation of dust, which is removed by dust extraction systems.

**Table 2** Elemental composition of burnt molding earth, wt.%

Si	O	Al	Fe	Mg	Ca	K	Mn
55.2 ± 5.7	34.4 ± 3.7	3.9 ± 0.7	3.0 ± 0.6	1.7 ± 0.3	1.0 ± 0	0.6 ± 0.3	0.2 ± 0.2

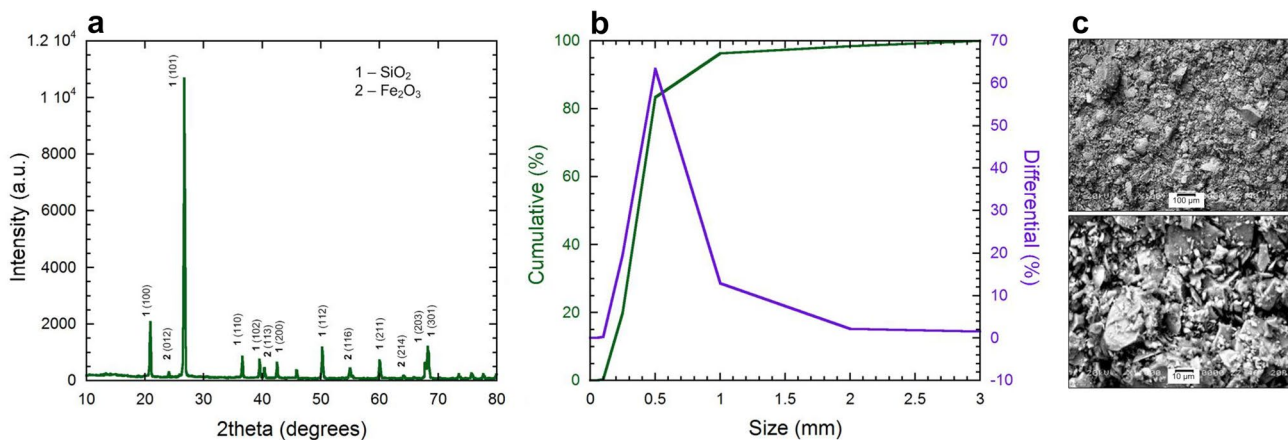


**Fig. 2** X-ray diffractogram (a), integral particle distribution curve (b), and SEM image of the sample of burnt molding earth (c)

**Table 3** Experimental data to determine the average grain size and coefficient homogeneity of finely dispersed fraction SFS

Sieve index	Size of the side of the sieve cell, d, mm	Fraction size, $\delta$ , mm	Residue on the sieve		The fraction of the mass of particles with a size smaller than the sides of the sieve cell, %
			g	%	
3	3	–	0	0	100
2	2	2.5 (2–3)	7.89	1.58	98.42
1	1	1.5 (1–2)	10.68	2.14	96.28
05	0.5	0.75 (0.5–1)	64.4	12.88	83.40
025	0.25	0.375 (0.25–0.5)	317.17	63.43	19.97
01	0.1	0.175 (0.1–0.25)	98.13	19.63	0.34
0063	0.063	0.0825 (0.065–0.1)	1.30	0.26	0.08
Residue	–	(<0.063)	0.43	0.08	0
Total			500	100	–

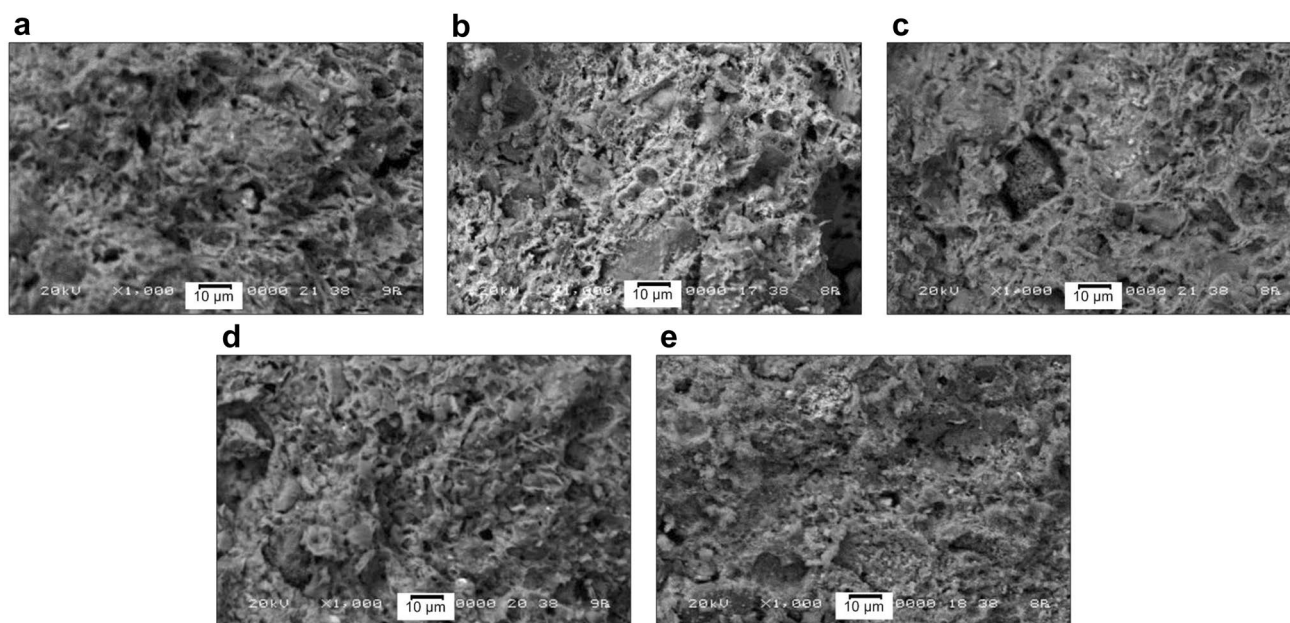
In the work, the grinding of SFS after its electromagnetic separation was carried out on a planetary mill. It was found that this produces about 24 wt.% finely dispersed fraction, the particles of which are characterized by a grain size of less than 190  $\mu\text{m}$ . This fraction cannot be returned to the technological process for the manufacture of casting molds.

### Analysis of obtained samples

The compositions of the samples and their properties are presented in Table 3.

The structure of test samples containing different amounts of finely dispersed fraction of burnt molding earth was studied using scanning microscopy (Fig. 3). The structure of all prototypes of ceramic bricks is characterized by a uniform distribution of pores, which ensures their high physical and

mechanical properties. In addition, samples containing 20 wt.% of the finely dispersed fraction of the molding burnt earth have a denser structure, which is also confirmed by their lower water absorption—10.78% (Table 4). However, from Table 4 it can be seen that with an increase in the content of the fine fraction of the molding burnt earth, the properties of ceramic bricks change slightly. Therefore, it is proposed to use 20 wt.% of the finely dispersed fraction of the burnt molding earth, i.e., completely replace the quartz sand with waste. This will recycle the largest amount of waste and save natural raw materials. Linear shrinkage, which were between 6.3 and 7.5%, decrease as SFS content increases. However, the linear shrinkage of ceramic brick containing 20 wt.% of SFS was larger than that of ceramic brick containing 15 wt.% of SFS (6.6% versus 6.3%, respectively). The obtained samples' water absorption ranges from 10.78 to 12.31 wt.%. Additionally,

**Fig. 3** Structure of ceramic bricks samples: 0% SFS (a); 5% SFS (b); 10% SFS (c); 15% SFS (d); 20% SFS (e)

**Table 4** Properties of ceramic bricks samples

Composition, wt.%			Shrinkage, %	Density, kg/m <sup>3</sup>	Water absorption, %	Compressive strength, MPa	Bending strength, MPa
Clay	Quartz sand	Fine-dispersed fraction of SFS					
80	20	–	7.0	2100	11.85	42.35	13.25
80	15	5	7.5	1990	12.31	39.15	12.52
80	10	10	6.9	2050	11.79	39.96	12.45
80	5	15	6.3	1980	11.17	40.12	13.14
80	–	20	6.6	2020	10.78	39.80	12.67

**Table 5** Properties of samples at different maximum firing temperature

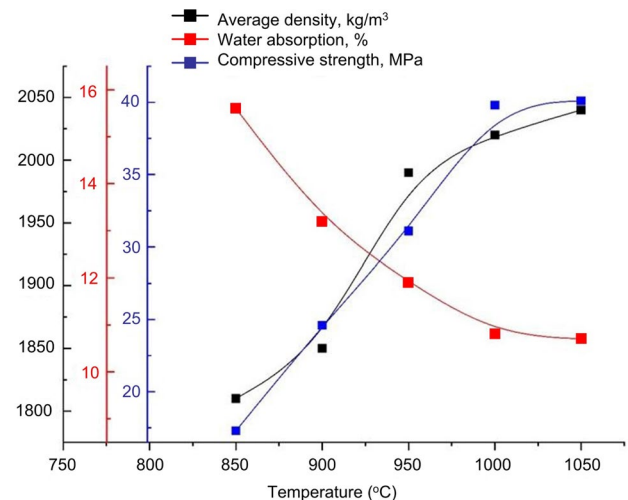
Maximum firing temperature, °C	Average density, kg/m <sup>3</sup>	Water absorption, %	Compressive strength, MPa	Comments
850	1810	15.6	17.3	Underburn
900	1850	13.2	24.6	Without defects
950	1990	11.9	31.1	Without defects
1000	2020	10.8	39.8	Without defects
1050	2040	10.7	40.1	Without defects
1100	–	–	–	Deformation of samples (overburning)

water absorption reduces as the SFS level raises. According to UNE-EN 772-11, the water absorption of standard products must be at least 6.0 weight percent, and for front products, it must be between 6.0 and 14.0 weight percent. All brick samples that were received meet UNE-EN 772-1 requirements and are suitable for use as standard products. The range of the compressive strength was in a range 39.15–42.35 MPa and bending strength 12.45–13.25 MPa. As the SFS content rises, the strength values drop. Each sample that was received satisfies the standard's strength requirements.

The final stage in the production of ceramic bricks is firing, which affects the quality of the resulting products. Therefore, further studies were carried out to determine the firing mode of ceramic bricks containing 80 wt.% clay and 20 wt.% finely dispersed fraction of SFS.

To select the maximum firing temperature, heat treatment of prototypes was carried out at temperatures from 850 to 1100 °C with an interval of 50 °C while raising the temperature at a rate of 175 °C/h and isothermal holding at the maximum temperature for an hour. For the samples obtained, the average density, water absorption and compressive strength were determined. The results of the experiment are presented in Table 4.

With an increase in the firing temperature to 1050 °C, the properties of the samples improve (Table 5, Fig. 4), and at 1100 °C, deformation of the samples is observed (ceramic burnout). As the temperature rises from 1000 to 1050 °C, the properties of the samples change

**Fig. 4** Properties of samples on the firing temperature

insignificantly, by less than 1%. Therefore, the firing temperature of 1000 °C was chosen as the optimal one.

Next, firing was carried out at a temperature of 1000 °C with isothermal exposure for 30, 60, 90, and 120 min (lines 1, 2, 3, and 4 in Fig. 5, respectively). For the samples obtained, the average density, water absorption, and ultimate compressive strength were also determined (Table 5).

As can be seen from Table 6, with isothermal exposure for 120 min, there is some deterioration in the properties of the samples, and their slight curvature (partial

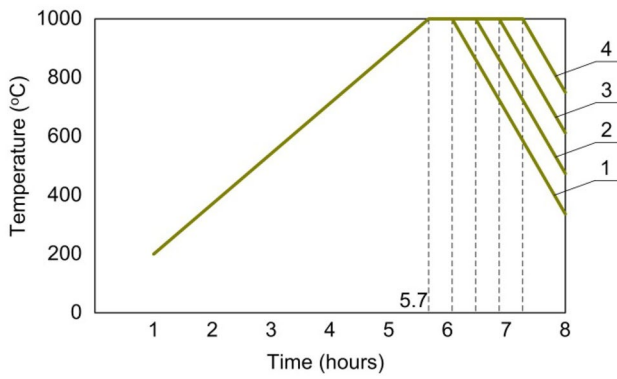


Fig. 5 Mode plot of firing

Table 6 Physical and mechanical properties of samples at different isothermal exposure at 1000 °C

Holding time, min	Density, kg/m <sup>3</sup>	Water absorption, %	Compressive strength, MPa	Comments
30	1980	12.4	33.5	Underburned
60	2020	10.8	39.8	Without defects
90	2010	10.8	40.2	Without defects
120	1990	10.7	40.5	Partially burnout

burnout) is also observed. At an isothermal holding time of 30 min, underburning occurs, as evidenced by low values of density and compressive strength, as well as an increased value of water absorption. The best properties of the prototypes are observed with isothermal exposure for 60–90 min. Since the properties of the samples practically

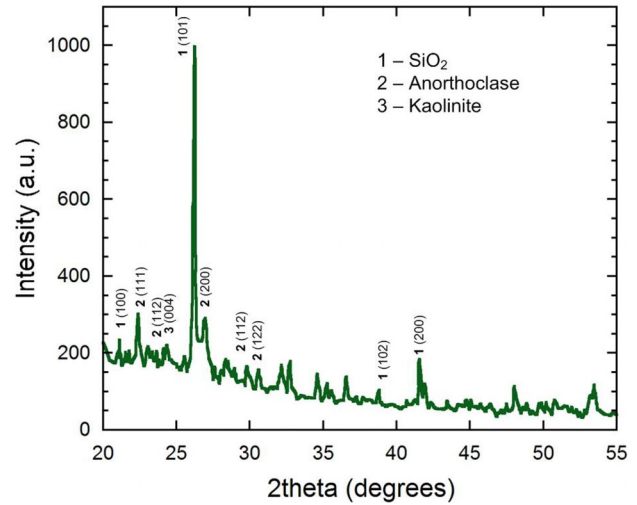


Fig. 6 X-ray diffractogram of ceramic brick containing 80 wt.% clay and 20 wt.% fine fraction of burnt molding earth, fired at temperature 1000 °C with isothermal exposure for 60 min

do not change in this interval, taking into account the need to save energy resources, it is proposed to carry out firing with isothermal exposure for 60 min. Thus, for a ceramic brick containing 80 wt.% clay and 20 wt.% finely dispersed fraction of molding burnt earth, firing at a temperature of 1000 °C with isothermal holding for 60 min was selected.

The diffraction patterns of the fired sample show the predominant content of quartz with a hexagonal structure with space groups *P3221* and characteristic peak (101) at 26.64 2theta; anorthoclase phase with an anorthic structure with space groups *P-1* and characteristic peaks at 21.85, 23.65, 24.25, 27.54, 26.65, 27.68, and 27.96 2theta (Fig. 6).

Table 7 compares the obtained results with previously published studies showing the promise of using a

Table 7 Comparison of obtained results with published analogs

Composition	Firing temperature, °C	Firing time, hours	Density, g/cm <sup>3</sup>	Water absorption, %	Compressive strength, MPa	References
Wood pulp 8%						
Clay 72% SFS 20%	850	1	1.75	11	3.03–3.5	[26]
Clay 70% SFS 30%	900	12	1.76	20.49	3.95	[27]
Paper pulp 8%						
Clay 62% SFS 30%	850	n/a	2.67	12.7	n/a	[28]
Clay 80% SFS 20%	850 950 1050	3.5	n/a n/a 2.015	13.0 11.1 8.1–8.7	n/a n/a 11–17	[29]
Clay 80% Finely dispersed fraction SFS 20%	1000	1	2.02	10.8	39.8	This work

finely dispersed fraction of the burnt molding earth in the production of ceramic bricks at relatively low firing temperatures.

By comparing the results of the measured parameters of the obtained samples with the results of published studies, the following conclusions can be drawn. The addition of 8% wood [38] or paper pulp [39], or the addition 20 [40] or 30% of SPS [41] and firing the mixture at 850–900 °C leads to a decrease in compressive strength and an increase in water absorption.

## Conclusions

The conducted studies confirm the possibility of complex processing of finely dispersed fraction SFS, which is a waste of foundry production. The finely dispersed fraction of SFS, which is formed in the process of its regeneration, is proposed to be used in the production of ceramic bricks as a lean additive.

The obtained samples of ceramic bricks containing 20 wt.% finely dispersed fraction of SFS were characterized by the following properties: average density 2020 kg/m<sup>3</sup>, water absorption 10.8%, compressive strength 39.8 MPa, flexural strength 12.67 MPa, which corresponds to the M300 brick grade according to GOST 530-2012 and to the standard UNE-EN 772. Samples of ceramic bricks containing finely dispersed fraction SFS were obtained at different isothermal exposure at low temperature of 1000 °C. However, it should be noted that, in general, with the addition of SPG up to 20 wt %, the values of the parameters of the samples did not change significantly.

The presented approach will reduce the impact of foundry production on the environment by preventing the disposal of the waste in question at landfills, expand the raw material base of the building materials industry and obtain high-quality products—ceramic bricks that meet the requirements of the standards.

**Author contributions** VZ: Conceptualization. Formal analysis. Investigation. Methodology. Resources. Supervision. Data curation. Validation. Writing—original draft. Writing—review and editing; VC: Formal analysis. Investigation. Data curation. Validation; VR: Formal analysis. Data curation. Validation. Visualization. Writing—original draft. Writing—review and editing.

**Funding** The authors received no funding from any source.

**Data availability** All data employed in support to the outcomes in the study are included in this article.

## Declarations

**Conflict of interest** The authors declare no competing interest with any previous work.

**Ethics approval and consent to participate** Not applicable.

**Consent for publication** Not applicable.

## References

1. Yefimenko N, Rajabzadeh M, Zaloga V, Fesenko D, Rysanaya O (2023) A Universal Quality Control System on Machine-Building Enterprises. In: *Grabchenko's International Conference on Advanced Manufacturing Processes* (pp. 391–399). Springer, Cham. [https://doi.org/10.1007/978-3-031-16651-8\\_37](https://doi.org/10.1007/978-3-031-16651-8_37)
2. Iqbal MF, Liu QF, Azim I, Zhu X, Yang J, Javed MF, Rauf M (2020) Prediction of mechanical properties of green concrete incorporating waste foundry sand based on gene expression programming. *J Hazard Mater* 384:121322. <https://doi.org/10.1016/j.jhazmat.2019.121322>
3. Iqbal MF, Liu QF, Azim I (2019) Experimental study on the utilization of waste foundry sand as embankment and structural fill. In: *IOP conference series: materials science and engineering* (Vol. 474, No. 1, p. 012042). IOP Publishing. <https://doi.org/10.1088/1757-899X/474/1/012042>
4. Aftab B, Ok YS, Cho J, Hur J (2019) Targeted removal of organic foulants in landfill leachate in forward osmosis system integrated with biochar/activated carbon treatment. *Water Res* 160:217–227. <https://doi.org/10.1016/j.watres.2019.05.076>
5. Mymrin V, Ribas HE, Pedroso DE, Pedroso CL, Klitzke W, Avanci MA, Goncalves AJ, Rolim PH (2022) Physical–chemical processes of sustainable materials' production from hazardous toner waste, galvanic glass waste and spent foundry sand. *J Mater Cycles Waste Manage* 25:396–406. <https://doi.org/10.1007/s10163-022-01557-9>
6. Akinwande AA, Balogun OA, Danso H, Romanovski V, Ademati AO, Oyediran AO (2023) Development of insulating masonry bricks from wood fiber and varying milled glass proportion. *J Civil Eng Constr* 12(1):40–54. <https://doi.org/10.32732/jceec.2023.12.1.40>
7. Barnabas AA, Balogun OA, Akinwande AA, Ogbodo JF, Ademati AO, Dongo EI, Romanovski V (2023) Reuse of walnut shell waste in the development of fired ceramic bricks. *Environ Sci Pollut Res* 30(5):11823–11837. <https://doi.org/10.1007/s11356-022-22955-4>
8. Abdulwahid MY, Akinwande AA, Kamarou M, Romanovski V, Al-Qasem IA (2023) The production of environmentally friendly building materials out of recycling walnut shell waste: a brief review. *Biomass Convers Biorefinery*. <https://doi.org/10.1007/s13399-023-04760-2>
9. Kamarou M, Moskovskikh D, Chan HL, Wang H, Li T, Akinwande AA, Romanovski V (2023) Low energy synthesis of anhydrite cement from waste lime mud. *J Chem Technol Biotechnol* 98:789–796. <https://doi.org/10.1002/JCTB.7284>
10. Romanovski V, Klyndyuk A, Kamarou M (2021) Green approach for low-energy direct synthesis of anhydrite from industrial wastes of lime mud and spent sulfuric acid. *J Environ Chem Eng* 9(6):106711. <https://doi.org/10.1016/j.jece.2021.106711>
11. Zalyhina V, Cheprasova V, Romanovski V (2022) Paper industry slag for the production of building ceramics. *J Chem Technol Biotechnol* 97(11):3091–3099. <https://doi.org/10.1002/JCTB.7174>
12. Romanovski V, Zhang L, Su X, Smorokov A, Kamarou M (2022) Gypsum and high quality binders derived from water treatment sediments and spent sulfuric acid: chemical engineering and environmental aspects. *Chem Eng Res Des* 184:224–232. <https://doi.org/10.1016/j.cherd.2022.06.008>
13. Kamarou M, Korob N, Hil A, Moskovskikh D, Romanovski V (2021) Low-energy technology for producing anhydrite in the CaCO<sub>3</sub> – H<sub>2</sub>SO<sub>4</sub> – H<sub>2</sub>O system derived from industrial wastes. *J*



- Chem Technol Biotechnol 96(7):2065–2071. <https://doi.org/10.1002/jctb.6740>
14. Romanovski V, Su X, Zhang L, Paspelau A, Smorokov A, Sehat AA, Akinwande AA, Korob N, Kamarou M (2023) Approaches for filtrate utilization from synthetic gypsum production. *Environ Sci Pollut Res*. <https://doi.org/10.1007/s11356-022-24584-3>
  15. Akinwande AA, Folorunso DO, Balogun OA, Romanovski V (2022) Mathematical modelling, multi-objective optimization, and compliance reliability of paper-derived eco-composites. *Environ Sci Pollut Res* 29(1):70135–70157. <https://doi.org/10.1007/s11356-022-20714-z>
  16. Akinwande AA, Balogun OA, Romanovski V (2022) Modeling, multi-response optimization, and performance reliability of green metal composites produced from municipal wastes. *Environ Sci Pollut Res*. <https://doi.org/10.1007/s11356-022-20023-5>
  17. Ademati AO, Akinwande AA, Balogun OA, Romanovski V (2022) Optimization of bamboo-fiber-reinforced composite-clay bricks for development of low-cost farm-settlements towards boosting rural agri-business in Africa. *J Mater Civ Eng* 34(12):04022335. [https://doi.org/10.1061/\(ASCE\)MT.1943-5533.0004489](https://doi.org/10.1061/(ASCE)MT.1943-5533.0004489)
  18. Akinwande AA, Balogun OA, Romanovski V, Danso H, Kamarou M, Ademati AO (2022) Mechanical performance and Taguchi optimization of kenaf fiber/cement-paperboard composite for interior application. *Environ Sci Pollut Res* 29:52675–52688. <https://doi.org/10.1007/s11356-022-19449-8>
  19. Akinwande AA, Balogun OA, Romanovski V, Ademati AO, Adetula YV (2022) Recycling of synthetic waste wig fiber in the production of cement-adobe for building envelope: physio-hydric properties. *Environ Sci Pollut Res* 29:34075–34091. <https://doi.org/10.1007/s11356-022-18649-6>
  20. Zalyhina V, Cheprasova V, Romanovski V (2021) Pigments from spent chloride-ammonium zinc plating electrolytes. *J Chem Technol Biotechnol* 96(10):2767–2774. <https://doi.org/10.1002/jctb.6822>
  21. Zalyhina V, Cheprasova V, Belyaeva V, Romanovski V (2021) Pigments from spent Zn, Ni, Cu, and Cd electrolytes from electroplating industry / *Environmental Science and Pollution*. Research 28:32660–32668. <https://doi.org/10.1007/s11356-021-13007-4>
  22. Martsul VN, Zalygina OS, Shibeka LA, Likhacheva AV, Ramanouski VI (2012) Some applications of galvanic manufacture waste/ *Proceedings of BSTU. Chemistry and technology of inorganic substances*. Vol. 3, pp 66–70
  23. Martsul VN, Likhacheva AV, Shibeka LA, Zalygina OS, Ramanouski VI, Khodin VV (2012) Inventory of galvanic sludge and deposits of the treatment facilities formed at the enterprises of the Republic of Belarus. In: *Proceedings of BSTU. Chemistry and technology of inorganic substances*. 3; pp 71–77
  24. Martsul VN, Zalygina OS, Likhacheva AV, Romanovski VI (2013) Treatment of electroplating shop wastewater at enterprises of the Republic of Belarus. In: *Proceedings of BSTU. Chemistry and technology of inorganic substances*. Vol. 3, pp 57–62
  25. Matsukevich I, Kulnich N, Romanovski V (2022) Direct reduced iron and zinc recovery from electric arc furnace dust. *J Chem Technol Biotechnol* 97(11):3091–3099. <https://doi.org/10.1002/jctb.7205>
  26. Hurynovich A, Kwietniewski M, Romanovski V (2021) Evaluation of the possibility of utilization of sewage sludge from Wastewater Treatment Plant – case study. *Desalin Water Treat* 227:16–25. <https://doi.org/10.5004/dwt.2021.27199>
  27. Smorokov A, Kantaev A, Bryankin D, Miklashevich A, Kamarou M, Romanovski V (2023) Low-temperature method for desilicization of polymetallic slags by ammonium bifluoride solution. *Environ Sci Pollut Res* 30(5):30271–30280. <https://doi.org/10.1007/s11356-022-24230-y>
  28. Smorokov A, Kantaev A, Bryankin D, Miklashevich A, Kamarou M, Romanovski V (2023) A novel low-energy approach of leucoxene concentrate desilicization by ammonium bifluoride solutions. *J Chem Technol Biotechnol* 98(3):726–733. <https://doi.org/10.1002/jctb.7277>
  29. Smorokov A, Kantaev A, Bryankin D, Miklashevich A, Kamarou M, Romanovski V (2022) Low-temperature desilicization of activated zircon concentrate by NH<sub>4</sub>HF<sub>2</sub> solution. *Miner Eng* 189:107909. <https://doi.org/10.1016/j.mineng.2022.107909>
  30. Sithole NT, Tsotetsi NT, Mashifana T, Sillanpää M (2022) Alternative cleaner production of sustainable concrete from waste foundry sand and slag. *J Clean Prod* 336:130399. <https://doi.org/10.1016/j.jclepro.2022.130399>
  31. Priyadarshini M, Giri JP (2022) Use of recycled foundry sand for the development of green concrete and its quantification. *J Build Eng* 52:104474. <https://doi.org/10.1016/j.job.2022.104474>
  32. Cunha S, Costa D, Aguiar JB, Castro F (2023) Mortars with the incorporation of treated ceramic molds shells wastes. *Constr Build Mater* 365:130074. <https://doi.org/10.1016/j.conbuildmat.2022.130074>
  33. Gautam L, Jain JK, Jain A, Kalla P (2022) Valorization of bone-china ceramic powder waste along with granite waste in self-compacting concrete. *Constr Build Mater* 315:125730. <https://doi.org/10.1016/j.conbuildmat.2021.125730>
  34. Schwarz M, Salva J, Vanek M, Poništ J, Prepilková V, Lobotková M, Turčániová E (2022) Assessment of possibilities of using waste foundry sand—review. *Int J Mater Res* 1:1
  35. Cioli F, Abbà A, Alias C, Sorlini S (2022) Reuse or disposal of waste foundry sand: an insight into environmental aspects. *Appl Sci* 12(13):6420. <https://doi.org/10.3390/app12136420>
  36. Anjum F, Naz MY, Ghaffar A, Kamran K, Shukrullah S, Ullah S (2022) Sustainable insulating porous building materials for energy-saving perspective: stones to environmentally friendly bricks. *Constr Build Mater* 318:125930. <https://doi.org/10.1016/j.conbuildmat.2021.125930>
  37. Filippenkov AA, Maizel SG, Afonaskin AV, Churkin BS, Hoffman EB, Churkin AB, Kategorenko A, Yu I (Ed.) Milyaev VM (Ed.) (2018). *Foundry technology: textbook*. (2nd ed., revised and supplemented ed.) Russian State Vocational Pedagogical University. ISBN 978-5-8050-0641-9
  38. Quijorna N, Coz A, Andres A, Cheeseman C (2012) Recycling of Waelz slag and waste foundry sand in red clay bricks. *Resour Conserv Recycl* 65:1–10. <https://doi.org/10.1016/j.resconrec.2012.05.004>
  39. Alonso-Santurde R, Andrés A, Viguri JR, Raimondo M, Guarini G, Zanelli C, Dondi M (2011) Technological behaviour and recycling potential of spent foundry sands in clay bricks. *J Environ Manage* 92(3):994–1002. <https://doi.org/10.1016/j.jenvman.2010.11.004>
  40. Alonso-Santurde R, Coz A, Viguri JR, Andrés A (2012) Recycling of foundry by-products in the ceramic industry: green and core sand in clay bricks. *Constr Build Mater* 27(1):97–106. <https://doi.org/10.1016/j.conbuildmat.2011.08.022>
  41. Hossiney N, Das P, Mohan MK, George J (2018) In-plant production of bricks containing waste foundry sand—a study with Belgaum foundry industry. *Case Stud Constr Mater* 9:e00170. <https://doi.org/10.1016/j.cscm.2018.e00170>

**Publisher's Note** Springer Nature remains neutral with regard to jurisdictional claims in published maps and institutional affiliations.

Springer Nature or its licensor (e.g. a society or other partner) holds exclusive rights to this article under a publishing agreement with the author(s) or other rightsholder(s); author self-archiving of the accepted manuscript version of this article is solely governed by the terms of such publishing agreement and applicable law.